Available online at www.sciencedirect.com
SCIENCE DIRECT®
International Journal of Solids and Structures 43 (2006) 5247–5266
INTERNATIONAL JOURNAL OF SOLIDS and STRUCTURES
www.elsevier.com/locate/ijsolstr

Imperfection sensitivity of the post-buckling behavior of higher-order shear deformable functionally graded plates

J. Yang [a,*], K.M. Liew [b], S. Kitipornchai [a]

[a] Department of Building and Construction, City University of Hong Kong, Tat Chee Avenue, Kowloon, Hong Kong
[b] Nanyang Centre for Supercomputing and Visualisation, School of Mechanical and Production Engineering, Nanyang Technological University, Nanyang Avenue, Singapore 639798, Singapore

Received 20 April 2005; received in revised form 22 June 2005
Available online 18 August 2005

Abstract

This paper investigates the sensitivity of the post-buckling behavior of shear deformable functionally graded plates to initial geometrical imperfections in general modes. A generic imperfection function that takes the form of the product of trigonometric and hyperbolic functions is used to model various possible initial geometrical imperfections such as sine type, local type, and global type imperfections. The formulations are based on Reddy's higher-order shear deformation plate theory and von Karman-type geometric nonlinearity. A semi-analytical method that makes use of the one-dimensional differential quadrature method, the Galerkin technique, and an iteration process is used to obtain the post-buckling equilibrium paths of plates with various boundary conditions that are subjected to edge compressive loading together with a uniform temperature change. Special attention is given to the effects of imperfection parameters, which include half-wave number, amplitude, and location, on the post-buckling response of plates. Numerical results presented in graphical form for zirconia/aluminum (ZrO_2/Al) graded plates reveal that the post-buckling behavior is very sensitive to the L2-mode local type imperfection. The influences of the volume fraction index, edge compression, temperature change, boundary condition, side-to-thickness ratio and plate aspect ratio are also discussed.

Keywords: Postbuckling; Functionally graded plate; Geometrical imperfection; Sensitivity; Higher-order shear deformation plate theory

1. Introduction

Composite plates are widely used in aerospace, automotive, marine and civil structures. The accurate prediction of the post-buckling response of these plates is of utmost importance in engineering design,

* Corresponding author. Tel.: +852 2194 2895; fax: +852 2788 7612.
E-mail address: jyang2@cityu.edu.hk (J. Yang).

0020-7683/$ - see front matter © 2005 Elsevier Ltd. All rights reserved.
doi:10.1016/j.ijsolstr.2005.06.061

because they are often subjected to in-plane loads, such as edge compression, that may result in nonlinear deformation at high load levels. It is well accepted that these structures possess unavoidable initial geometrical imperfections that may be globally or locally distributed and may substantially affect the post-buckling behavior of plates. Quite a few post-buckling analyses of imperfect composite plates have been conducted, notably those by Yamaki (1959), Hui (1986), Librescu and Souza (1993), Dawe et al. (1995), Librescu et al. (1995), Shen and Williams (1997), Shen (1998, 1999, 2000, 2001), Yang and Zhang (2000), Featherston (2001), Yang et al. (2001), Zou and Qiao (2002), Zou and Lam (2003) and Girish and Ramachandra (2005). However, most of these studies are based on the simplified assumption that the initial geometrical imperfection has a similar form to the deformed shape of the plate, and the investigations dealing with general geometrical imperfections are limited in number. This is partly due to the lack of sufficient information about the exact size and shape of the actual imperfections to be discussed. Kapania and Yang (1987) treated general imperfections with polynomials as simulation functions and analyzed the compressive post-buckling of isotropic rectangular plates. This approach was used by Liu and Lam (2001), who presented finite strip solutions for imperfect composite laminated plates based on the classical plate theory (CPT). Using a model that bases the form of the imperfection on the first bifurcational eigenmode or a superposition of several bifurcational eigenmodes, Featherston (2001) gave a finite element analysis of the imperfection sensitivity of the post-buckling behavior of flat plates under a combined action of edge compression and shear. The effects of imperfection shape and amplitude were discussed in detail through comprehensive numerical examples.

In the past few years, the use of functionally graded materials (FGMs) has gained intensive attention in many engineering applications (Ichikawa, 2000). A typical FGM is an inhomogeneous composite that is usually made from a mixture of ceramic and metal with both the compositional profile and material properties varying smoothly with respect to the spatial coordinates. Although a number of metallurgical techniques have been developed for the fabrication of bulk FGMs, the complexity of the manufacturing process means that geometrical imperfections, such as initial curvatures, are inevitable.

Many buckling and post-buckling analyses of perfect, purely FGM or FGM laminated plates have been reported. Among those, studies concerning the linear stability of FGM plates including compressive buckling, thermal buckling and buckling of initially stressed plates have been conducted by, for example, Feldman and Aboudi (1997), Javaheri and Eslami (2002), Morimoto et al. (2003), Liew et al. (2003, 2004), Chen and Liew (2004), Na and Kim (2004) and Najafizadeh and Heydari (2004). Most recently, Yang et al. (2005) extended their deterministic work on FGMs to the buckling of FGM plates with randomness in material properties and presented second-order statistics for the critical buckling load of zirconia/aluminum FGM rectangular plates. The post-buckling of FGM plates under compressive loads with or without lateral pressure was examined by Yang and Shen (2003) and Ma and Wang (2003a). Ma and Wang (2003b), Woo et al. (2003) and Liew et al. (2004) dealt with the post-buckling characteristics of FGM plates under combined thermo-mechanical loading. Liew et al. (2003) also studied the post-buckling behavior of FGM plates integrated with surface-mounted piezoelectric actuators and subjected to in-plane forces, a uniform temperature change, and a constant applied actuator voltage. The linear and nonlinear instability of FGM plates under various thermo-electro-mechanical loading conditions were addressed as subset problems. All of the aforementioned works dealt with perfect plate structures only, and the effect of geometrical imperfections has not been accounted for. The only two exceptions are the papers by Yang and Shen (2003) and Liew et al. (2004), in which the assumption that the imperfection has a form that is similar to the deflected shape of the plate was adopted. As far as the authors are aware, no previous work has been undertaken on the post-buckling behavior of FGM plates with general mode imperfections.

This paper investigates the nonlinear behavior of imperfect shear deformable functionally graded rectangular plates in the post-buckling phase. Attention is focused on the effects of different imperfection parameters, which include the imperfection half-wave number, amplitude, and location, on the post-buckling characteristics of plates under a combined action of edge compression and a uniform temperature

change. Instead of assuming the imperfection mode to be the same as the deformed shape, a variety of sine type, local type, and global type imperfections are considered by employing a generic imperfection function that was developed by the present authors (Kitipornchai et al., 2004) from the one-dimensional imperfection model for struts (Wadee, 2000). The formulation is based on Reddy's higher-order shear deformation plate theory (HSDPT) (Reddy, 1984). A semi-analytical approach and an iteration procedure are used to determine the post-buckling equilibrium path for graded plates. Numerical results are presented for ZrO_2/Al graded plates in graphical form. A detailed discussion concerning the influence of the geometrical imperfection mode as well as other system parameters on the post-buckling response is presented.

2. Theoretical formulations

Consider an imperfect rectangular plate that is made of ceramic/metal functionally graded materials of length a, width b and thickness h and defined in a Cartesian coordinate system (x, y, z) as shown in Fig. 1, where (x, y) are the coordinates of a point in the mid-plane of the plate and z is a coordinate perpendicular to the mid-plane and points upwards. It is assumed that the material composition of the plate varies smoothly along the thickness direction only in terms of volume fractions according to a power law distribution

$$V_c(z) = \left(\frac{2z+h}{2h}\right)^n, \qquad V_m(z) = 1 - \left(\frac{2z+h}{2h}\right)^n \tag{1}$$

where $V(z)$ represents the volume fraction of the material phase involved, n is a non-negative volume fraction index, and the subscripts "c" and "m" stand for ceramic and metal. It is evident from Eq. (1) that the upper surface of the plate ($z = h/2$) is purely ceramic, and the lower surface ($z = -h/2$) is purely metallic. The local effective material properties P_{eff}, such as Young's modulus E and coefficient of linear thermal expansion α, at a given point can be estimated through

$$P_{eff} = P_m V_m + P_c V_c \tag{2}$$

and Poisson's ratio v is assumed to be a constant for simplicity.

Suppose that the plate is initially stress free at temperature T_0 and is then subjected to a uniform temperature change ΔT and uniform edge compressive loads p_x along the x-axis and p_y along the y-axis. In accordance with Reddy's higher-order shear deformation plate theory (Reddy, 1984), the displacement field of an arbitrary point within the plate domain is assumed to be

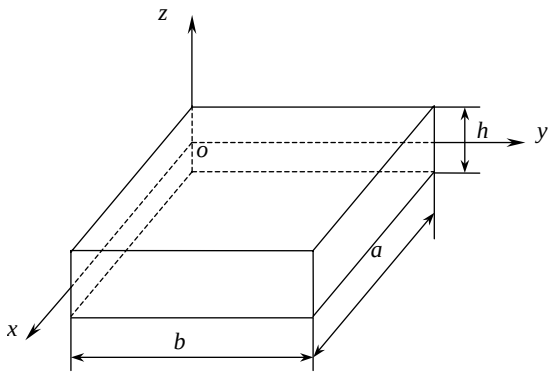

Fig. 1. An FGM rectangular plate and its coordinate system.

$$\overline{U} = U(x,y) + z\Psi_x(x,y) - c_1 z^3\left(\Psi_x(x,y) + \frac{\partial \overline{W}}{\partial x}\right) \tag{3a}$$

$$\overline{V} = V(x,y) + z\Psi_y(x,y) - c_1 z^3\left(\Psi_y(x,y) + \frac{\partial \overline{W}}{\partial y}\right) \tag{3b}$$

$$\overline{W} = W(x,y) + W^*(x,y) \tag{3c}$$

where $c_1 = 4/3h^2$, $(\overline{U}, \overline{V}, \overline{W})$ are the displacements of an arbitrary point within the plate, (U, V, W) are the additional mid-plane displacement components that are caused by thermo-mechanical loading, Ψ_x and Ψ_y are the slope rotations in the x–z and y–z planes, and W^* is the initial geometrical imperfection.

In this study, a generic model developed from the one-dimensional imperfection function for struts (Wadee, 2000) is used to simulate various possible imperfection modes that may be either highly localized or globally distributed. The model takes the form of the products of trigonometric and hyperbolic functions as

$$W^* = \eta h \operatorname{sech}\left[\delta_1(\xi - \psi_1)\right] \cos\left[\mu_1 \pi(\xi - \psi_1)\right] \operatorname{sech}\left[\delta_2(\zeta - \psi_2)\right] \cos\left[\mu_2 \pi(\zeta - \psi_2)\right] \tag{4}$$

where $\xi = x/a$, $\zeta = y/b$, η is the dimensionless maximum amplitude of the initially deflected geometry, δ_1 and δ_2 are the constants that define the degree of localization of the imperfection that is symmetric about $\xi = \psi_1$ and $\zeta = \psi_2$, and μ_1 and μ_2 are the half-wave numbers of the imperfection in the x-axis and y-axis, respectively. This model was first proposed by the authors (Kitipornchai et al., 2004), and is capable of modeling a wide range of initial imperfection modes, which include sine type imperfections when $\delta_1 = \delta_2 = 0$, $\mu_1 = \mu_2 = 1$, $\psi_1 = \psi_2 = 0.5$; local type imperfections when $\delta_1 \neq 0$, $\delta_2 \neq 0$; and global type imperfections when $\delta_1 = \delta_2 = 0$, $\mu_1 \neq 1$ or $\mu_2 \neq 1$.

The equations of equilibrium of an imperfect FGM plate, in the absence of body forces, are

$$\frac{\partial N_x}{\partial x} + \frac{\partial N_{xy}}{\partial y} = 0 \tag{5}$$

$$\frac{\partial N_{xy}}{\partial x} + \frac{\partial N_y}{\partial y} = 0 \tag{6}$$

$$\begin{aligned}&\frac{\partial Q_x}{\partial x} + \frac{\partial Q_y}{\partial y} - 3c_1\left(\frac{\partial R_x}{\partial x} + \frac{\partial R_y}{\partial y}\right) + c_1\left(\frac{\partial^2 P_x}{\partial x^2} + 2\frac{\partial^2 P_{xy}}{\partial x \partial y} + \frac{\partial^2 P_y}{\partial y^2}\right) + \frac{\partial}{\partial x}\left(N_x \frac{\partial (W + W^*)}{\partial x} + N_{xy}\frac{\partial (W + W^*)}{\partial y}\right)\\ &\quad + \frac{\partial}{\partial y}\left(N_{xy}\frac{\partial (W + W^*)}{\partial x} + N_y \frac{\partial (W + W^*)}{\partial y}\right) = 0\end{aligned} \tag{7}$$

$$\frac{\partial M_x}{\partial x} + \frac{\partial M_{xy}}{\partial y} - Q_x + 3c_1 R_x - c_1\left(\frac{\partial P_x}{\partial x} + \frac{\partial P_{xy}}{\partial y}\right) = 0 \tag{8}$$

$$\frac{\partial M_{xy}}{\partial x} + \frac{\partial M_y}{\partial y} - Q_y + 3c_1 R_y - c_1\left(\frac{\partial P_{xy}}{\partial x} + \frac{\partial P_y}{\partial y}\right) = 0 \tag{9}$$

The stress resultants $\mathbf{N} = [N_x, N_y, N_{xy}]'$, $\mathbf{Q} = [Q_y, Q_x]'$, $\mathbf{R} = [R_y, R_x]'$, moment resultants $\mathbf{M} = [M_x, M_y, M_{xy}]'$ and $\mathbf{P} = [P_x, P_y, P_{xy}]'$, where "′" indicates transposition of a matrix, are defined by

$$\begin{Bmatrix} \mathbf{N} \\ \mathbf{M} \\ \mathbf{P} \end{Bmatrix} = \begin{bmatrix} \mathbf{A} & \mathbf{B} & \mathbf{E} \\ \mathbf{B} & \mathbf{D} & \mathbf{F} \\ \mathbf{E} & \mathbf{F} & \mathbf{H} \end{bmatrix} \begin{Bmatrix} \boldsymbol{\varepsilon}^{(0)} \\ \boldsymbol{\varepsilon}^{(1)} \\ \boldsymbol{\varepsilon}^{(3)} \end{Bmatrix} + \begin{Bmatrix} \mathbf{N}^{\mathrm{T}} \\ \mathbf{M}^{\mathrm{T}} \\ \mathbf{P}^{\mathrm{T}} \end{Bmatrix}, \quad \begin{Bmatrix} \mathbf{Q} \\ \mathbf{R} \end{Bmatrix} = \begin{bmatrix} \tilde{\mathbf{A}} & \tilde{\mathbf{D}} \\ \tilde{\mathbf{D}} & \tilde{\mathbf{F}} \end{bmatrix} \begin{Bmatrix} \boldsymbol{\gamma}^{(0)} \\ \boldsymbol{\gamma}^{(2)} \end{Bmatrix} \tag{10}$$

among which the thermal stress and moment resultants are

$$\begin{bmatrix} N_x^{\mathrm{T}} & M_x^{\mathrm{T}} & P_x^{\mathrm{T}} \\ N_y^{\mathrm{T}} & M_y^{\mathrm{T}} & P_y^{\mathrm{T}} \\ N_{xy}^{\mathrm{T}} & M_{xy}^{\mathrm{T}} & P_{xy}^{\mathrm{T}} \end{bmatrix} = -\int_{-h/2}^{h/2} \begin{Bmatrix} (Q_{11}+Q_{12})\alpha \\ (Q_{11}+Q_{12})\alpha \\ 0 \end{Bmatrix} (1, z, z^3)\Delta T \, \mathrm{d}z \tag{11}$$

where Q_{ij} are the elastic constants for the functionally graded material

$$Q_{11} = Q_{22} = \frac{E}{1-\nu^2}, \quad Q_{12} = \frac{\nu E}{1-\nu^2}, \quad Q_{16} = Q_{26} = 0, \quad Q_{44} = Q_{55} = Q_{66} = \frac{E}{2(1+\nu)} \tag{12}$$

In Eq. (10), the stiffness components A_{ij}, B_{ij}, D_{ij}, E_{ij}, F_{ij}, and H_{ij} are calculated from

$$(A_{ij}, B_{ij}, D_{ij}, E_{ij}, F_{ij}, H_{ij}) = \int_{-h/2}^{h/2} Q_{ij}(1, z, z^2, z^3, z^4, z^6)\, \mathrm{d}z \quad (i, j = 1, 2, 6) \tag{13a}$$

$$(\tilde{A}_{ij}, \tilde{D}_{ij}, \tilde{F}_{ij}) = \int_{-h/2}^{h/2} Q_{ij}(1, z^2, z^4)\, \mathrm{d}z \quad (i, j = 4, 5) \tag{13b}$$

As the in-plane displacements are small compared with the transverse displacement and the higher-order strain terms are negligible, the von Karman-type nonlinear strains that are associated with the displacement field in Eq. (3) are obtained as

$$\begin{aligned}
\boldsymbol{\varepsilon}^{(0)} &= \begin{Bmatrix} \varepsilon_x^{(0)} \\ \varepsilon_y^{(0)} \\ \varepsilon_{xy}^{(0)} \end{Bmatrix} = \begin{Bmatrix} \dfrac{\partial U}{\partial x} + \dfrac{1}{2}\left(\dfrac{\partial W}{\partial x}\right)^2 + \dfrac{\partial W}{\partial x}\dfrac{\partial W^*}{\partial x} \\ \dfrac{\partial V}{\partial y} + \dfrac{1}{2}\left(\dfrac{\partial W}{\partial y}\right)^2 + \dfrac{\partial W}{\partial y}\dfrac{\partial W^*}{\partial y} \\ \dfrac{\partial U}{\partial y} + \dfrac{\partial V}{\partial x} + \dfrac{\partial W}{\partial x}\dfrac{\partial W}{\partial y} + \dfrac{\partial W^*}{\partial x}\dfrac{\partial W}{\partial y} + \dfrac{\partial W}{\partial x}\dfrac{\partial W^*}{\partial y} \end{Bmatrix}, \\
\boldsymbol{\varepsilon}^{(1)} &= \begin{Bmatrix} \varepsilon_x^{(1)} \\ \varepsilon_y^{(1)} \\ \varepsilon_{xy}^{(1)} \end{Bmatrix} = \begin{Bmatrix} \dfrac{\partial \Psi_x}{\partial x} \\ \dfrac{\partial \Psi_y}{\partial y} \\ \dfrac{\partial \Psi_y}{\partial x} + \dfrac{\partial \Psi_x}{\partial y} \end{Bmatrix}, \quad \boldsymbol{\varepsilon}^{(3)} = \begin{Bmatrix} \varepsilon_x^{(3)} \\ \varepsilon_y^{(3)} \\ \varepsilon_{xy}^{(3)} \end{Bmatrix} = c_1 \begin{Bmatrix} \dfrac{\partial \Psi_x}{\partial x} + \dfrac{\partial^2 W}{\partial x^2} + \dfrac{\partial^2 W^*}{\partial x^2} \\ \dfrac{\partial \Psi_y}{\partial y} + \dfrac{\partial^2 W}{\partial y^2} + \dfrac{\partial^2 W^*}{\partial y^2} \\ \dfrac{\partial \Psi_x}{\partial y} + \dfrac{\partial \Psi_y}{\partial x} + 2\dfrac{\partial^2 W}{\partial x \partial y} + 2\dfrac{\partial^2 W^*}{\partial x \partial y} \end{Bmatrix}, \\
\boldsymbol{\gamma}^{(0)} &= \begin{Bmatrix} \varepsilon_4^{(0)} \\ \varepsilon_5^{(0)} \end{Bmatrix} = \begin{Bmatrix} \Psi_y + \dfrac{\partial W}{\partial y} + \dfrac{\partial W^*}{\partial y} \\ \Psi_x + \dfrac{\partial W}{\partial x} + \dfrac{\partial W^*}{\partial x} \end{Bmatrix}, \quad \boldsymbol{\gamma}^{(2)} = \begin{Bmatrix} \varepsilon_4^{(2)} \\ \varepsilon_5^{(2)} \end{Bmatrix} = -3c_1 \begin{Bmatrix} \Psi_y + \dfrac{\partial W}{\partial y} + \dfrac{\partial W^*}{\partial y} \\ \Psi_x + \dfrac{\partial W}{\partial x} + \dfrac{\partial W^*}{\partial x} \end{Bmatrix}
\end{aligned} \tag{14}$$

Let Φ be related to the stress resultants by $N_x = \Phi_{,yy}$, $N_y = \Phi_{,xx}$, and $N_{xy} = -\Phi_{,xy}$, where a comma denotes partial differentiation with respect to the coordinates, and rewrite relationship (10) in partial reverse form as

$$\begin{Bmatrix} \boldsymbol{\varepsilon}^{(0)} \\ \mathbf{M} - \mathbf{M}^{\mathrm{T}} \\ \mathbf{P} - \mathbf{P}^{\mathrm{T}} \end{Bmatrix} = \begin{bmatrix} \mathbf{A}^* & \mathbf{B}^* & \mathbf{E}^* \\ -(\mathbf{B}^*)' & \mathbf{D}^* & (\mathbf{F}^*)' \\ -(\mathbf{E}^*)' & \mathbf{F}^* & \mathbf{H}^* \end{bmatrix} \begin{Bmatrix} \mathbf{N} - \mathbf{N}^{\mathrm{T}} \\ \boldsymbol{\varepsilon}^{(1)} \\ \boldsymbol{\varepsilon}^{(3)} \end{Bmatrix} \tag{15}$$

in which $(\,)'$ represents the transpose of the matrix, and the reduced plate stiffness components A_{ij}^*, B_{ij}^*, D_{ij}^*, E_{ij}^*, F_{ij}^*, H_{ij}^* are determined by

$$\mathbf{A}^* = \mathbf{A}^{-1}, \mathbf{B}^* = -\mathbf{A}^{-1}\mathbf{B}, \mathbf{D}^* = \mathbf{D} - \mathbf{B}\mathbf{A}^{-1}\mathbf{B}, \mathbf{E}^* = -\mathbf{A}^{-1}\mathbf{E}, \mathbf{F}^* = \mathbf{F} - \mathbf{E}\mathbf{A}^{-1}\mathbf{B}, \mathbf{H}^* = \mathbf{H} - \mathbf{E}\mathbf{A}^{-1}\mathbf{E} \tag{16}$$

Introducing the dimensionless quantities

$$\begin{aligned}
&\beta = a/b, \quad \Delta = (D_{11}^* D_{22}^* A_{11}^* A_{22}^*)^{1/4}, \quad \lambda_T = 100\alpha_c \Delta T, \\
&(w, w^*) = (W, W^*)/\Delta, \quad f = \Phi/(D_{11}^* D_{22}^*)^{1/2}, \quad (\psi_x, \psi_y) = (\Psi_x, \Psi_y)a/\Delta, \\
&\gamma_{14} = [D_{22}^*/D_{11}^*]^{1/2}, \quad \gamma_{24} = [A_{11}^*/A_{22}^*]^{1/2}, \quad (\lambda_x, \lambda_y) = (p_x b^2, p_y a^2)/(D_{11}^* D_{22}^*)^{1/2}
\end{aligned} \tag{17}$$

substituting Eqs. (14) and (15) into equilibrium Eqs. (5)–(9), and considering the conditions of the deformation compatibility of the plate leads to the nonlinear governing equations for an imperfect graded plate under edge compression and a uniform temperature change, expressed in terms of w, ψ_x, ψ_y, f, as follows

$$L_{11}(w) - L_{12}(\psi_x) - L_{13}(\psi_y) + \gamma_{14} L_{14}(f) = \gamma_{14}\beta^2 [L(w, f) + L(w^*, f)] \tag{18}$$

$$L_{21}(f) + \gamma_{24} L_{22}(\psi_x) + \gamma_{24} L_{23}(\psi_y) - \gamma_{24} L_{24}(w) = -\gamma_{24}\beta^2 \left[\frac{1}{2} L(w, w) + L(w^*, w)\right] \tag{19}$$

$$L_{31}(w) + L_{32}(\psi_x) - L_{33}(\psi_y) + \gamma_{14} L_{34}(f) = 0 \tag{20}$$

$$L_{41}(w) - L_{42}(\psi_x) + L_{43}(\psi_y) + \gamma_{14} L_{44}(f) = 0 \tag{21}$$

where the second terms in the right-hand side of Eqs. (18) and (19) reflect the contribution of the initial geometrical imperfection to the post-buckling response, the nonlinear partial differential operator $L(\,) = (\,)_{,\xi\xi}(\,)_{,\zeta\zeta} - 2(\,)_{,\xi\zeta}(\,)_{,\xi\zeta} + (\,)_{,\zeta\zeta}(\,)_{,\xi\xi}$, L_{ij} $(i, j = 1, \ldots, 4)$ are the linear partial differential operators. The dimensionless quantities not identified in Eq. (17) are given in Appendices A and B.

An FGM plate that is either simply supported (S) or clamped (C) at both edges $\zeta = 0$, 1, and may be simply supported (S), clamped (C), or free (F) at edges $\xi = 0$, 1 is considered. The associated out-of-plane boundary conditions at $\xi = 0$, 1 are

$$\text{Simply supported(S):} \quad w = M_x = \psi_y = P_x = 0 \tag{22a}$$

$$\text{Clamped(C):} \quad w = \psi_x = \psi_y = \frac{\partial w}{\partial \xi} = 0 \tag{22b}$$

$$\text{Free(F):} \quad Q_x^* = M_x = M_{xy}^* = P_x = 0 \tag{22c}$$

and those at $\zeta = 0$, 1 require that

$$\text{Simply supported(S):} \quad w = M_y = \psi_x = P_y = 0 \tag{23a}$$

$$\text{Clamped(C):} \quad w = \psi_y = \psi_x = \frac{\partial w}{\partial \zeta} = 0 \tag{23b}$$

Two different types of in-plane boundary conditions, categorized as "movable" and "immovable" depending on the in-plane displacement constraints, are considered in the present analysis and can be expressed in terms of stress function as

$$f_{,\xi\zeta} = 0, \quad f_{,ss} + \lambda_n = 0 \quad \text{(for movable edges)} \tag{24a}$$

or

$$f_{,\xi\zeta} = 0, \quad \delta_n = 0 \quad \text{(for immovable edges)} \tag{24b}$$

The subscripts "n" and "s" refer to the normal and tangential directions of the plate edge, Q_x^* and M_{xy}^* are the generalized transverse shear force and moment and δ_n is the end shortening, the dimensionless forms of which are given by Liew et al. (2003).

3. Solution method

A semi-analytical approach combined with an iteration process is used in the present analysis to study the post-buckling of the imperfect FGM plate. To begin with, we convert the partial differential governing Eqs. (18)–(21) and the associated boundary conditions at $\xi = 0, 1$ in Eqs. (22) and (24) into a set of ordinary differential equations by using the one-dimensional differential quadrature approximation in the ξ-axis

$$\boldsymbol{\chi} = [w, f, \psi_x, \psi_y], \quad \boldsymbol{\chi} = \sum_{j=1}^{N} \Theta_j(\xi)\chi_j, \quad \frac{\partial^k}{\partial \xi^k}\boldsymbol{\chi}|_{\xi=\xi_i} = \sum_{j=1}^{N} C_{ij}^{(k)}\boldsymbol{\chi}_j \tag{25}$$

where

$$\boldsymbol{\chi}_j = \boldsymbol{\chi}(\xi_j) = [w_j, f_j, \psi_{xj}, \psi_{yj}] \tag{26}$$

is the value of $\boldsymbol{\chi}$ at the jth nodal line, and N is the total number of nodal lines that are parallel to the ζ-axis and distributed along the ξ-axis according to a cosine spacing pattern with stable convergence characteristics,

$$\xi_j = \frac{1}{2}\left[1 - \cos\frac{\pi(j-1)}{N-1}\right] \quad (j = 1, 2, \ldots, N) \tag{27}$$

and $\Theta_j(\xi)$ is the Lagrange's interpolation polynomial

$$\Theta_j(\xi) = \frac{\Re(\xi)}{(\xi - \xi_j)\Re^{(1)}(\xi)}$$

$$\Re(\xi) = \prod_{i=1}^{N}(\xi - \xi_i), \quad \Re^{(1)}(\xi) = \prod_{i=1, i\neq j}^{N}(\xi_j - \xi_i) \tag{28}$$

The weighting coefficients $C_{ij}^{(k)}$ can be obtained using the following recurrence formula (Bert et al., 1993, 1998; Liew et al., 2001; Yang et al., 2004). For $i \neq j$

$$C_{ij}^{(k)} = k\left(C_{ii}^{(k-1)}C_{ij}^{(1)} - \frac{C_{ij}^{(k-1)}}{(\xi_i - \xi_j)}\right) \quad (i, j = 1,\ 2, \ldots N; \quad k = 2, 3, \ldots, N-1) \tag{29}$$

and for $i = j$

$$C_{ii}^{(k)} = -\sum_{j=1; i\neq j}^{N} C_{ij}^{(k)} \quad (i = 1,\ 2, \ldots N, \quad k = 1, 2, \ldots, N-1) \tag{30}$$

where the weighting coefficients of the first order derivatives $C_{ij}^{(1)}$ are

$$C_{ij}^{(1)} = \frac{\Re^{(1)}(\xi_i)}{(\xi_i - \xi_j)\Re^{(1)}(\xi_j)} \quad (i, j = 1, 2, \ldots, N) \tag{31}$$

Putting Eq. (25) into the partial differential governing Eqs. (18)–(21) and the associated boundary conditions (22) and (24) leads to a set of ordinary differential equations in terms of $\boldsymbol{\chi}_j$, the solution of which is expressed as

$$\boldsymbol{\chi}_j = \boldsymbol{\chi}_{j0} + \sum_{m=1}^{M} \boldsymbol{\chi}_{jm}\Phi_{jm} \tag{32}$$

in which

$$\boldsymbol{\chi}_{j0} = \left[0, -\frac{1}{2}\left(\zeta^2\lambda_x^* + \xi^2\lambda_y^*\right), 0, 0\right]$$
$$\boldsymbol{\Phi}_{jm} = \begin{bmatrix} a_{jm} & 0 & 0 & 0 \\ 0 & b_{jm} & 0 & 0 \\ 0 & 0 & c_{jm} & 0 \\ 0 & 0 & 0 & d_{jm} \end{bmatrix} \tag{33}$$

where M is the truncated number of series and a_{jm}, b_{jm}, c_{jm}, d_{jm} are the coefficients to be determined. It should be noted that λ_x^* and λ_y^* are due to the combined action of the applied in-plane forces (λ_x, λ_y) and the thermally induced reactions from immovable constraints, and can be determined from the different in-plane boundary conditions in Eq. (24). $\boldsymbol{\chi}_{jm}$ is composed of analytical functions w_{jm}, $\hat{f}_{jm}$, ψ_{xjm}, and ψ_{yjm} which satisfy all of the boundary conditions at edges $\zeta = 0$, 1 in Eqs. (23) and (24) and takes the form of

$$\begin{aligned}\boldsymbol{\chi}_{jm} &= [w_{jm}, \hat{f}_{jm}, \psi_{xjm}, \psi_{yjm}] \\ &= [\sin(m\pi\zeta), \sin\alpha_m\zeta - \sinh\alpha_m\zeta - \phi_m(\cos\alpha_m\zeta - \cosh\alpha_m\zeta), \sin(m\pi\zeta), \cos(m\pi\zeta)]\end{aligned} \tag{34a}$$

for plates that are simply supported at both $\zeta = 0$ and $\zeta = 1$, or

$$\begin{aligned}\boldsymbol{\chi}_{jm} = [w_{jm}, \hat{f}_{jm}, \psi_{xjm}, \psi_{yjm}] = [&\sin\alpha_m\zeta - \sinh\alpha_m\zeta - \phi_m(\cos\alpha_m\zeta - \cosh\alpha_m\zeta), \sin\alpha_m\zeta - \sinh\alpha_m\zeta \\ &- \phi_m(\cos\alpha_m\zeta - \cosh\alpha_m\zeta), \sin(m\pi\zeta), \sin(m\pi\zeta)]\end{aligned} \tag{34b}$$

for plates clamped at both $\zeta = 0$ and $\zeta = 1$, where $\phi_m = (\sin\alpha_m - \sinh\alpha_m)/(\cos\alpha_m - \cosh\alpha_m)$, $\alpha_m = (2m+1)\pi/2$.

Making use of relationships $r_x = \lambda_x/\lambda_p = p_x/p_0$ and $r_y = \lambda_y/\lambda_p = p_y/p_0$ with λ_p and p_0 serving as the dimensionless and dimensional in-plane load amplitudes, substituting expressions (32)–(34) into the ordinary differential equations and then employing Galerkin's procedure to minimize the interior residual gives a nonlinear algebraic system in matrix form as

$$\left(\mathbf{K}_0 + \mathbf{K}_0^* + \lambda_p\mathbf{K}_\lambda + \lambda_T\mathbf{K}_T + \mathbf{K}_{NL}(\tilde{\boldsymbol{\chi}})\right)\tilde{\boldsymbol{\chi}} = \mathbf{R}^T \tag{35}$$

where $\mathbf{K}_0$ is a constant coefficient matrix, $\mathbf{K}_0^*$ is a matrix showing the effect of initial geometrical imperfection, $\mathbf{K}_\lambda$ and $\mathbf{K}_T$ are the coefficient matrices associated with the applied in-plane edge forces and temperature change, $\mathbf{K}_{NL}$ is a nonlinear matrix that is dependent on the unknown vector $\tilde{\boldsymbol{\chi}}$ which consists of all of the unknown constants $\boldsymbol{\chi}_{jm}$ ($j = 1, \ldots, N$, $m = 1, \ldots, M$), $\mathbf{R}^T$ stands for the thermal load vector that comes from the stress-related boundary conditions in Eqs. (22)–(24).

It should be mentioned that this formulation is generic, and that Eq. (35) can be used to analyze several subset problems, such as the elastic buckling, compressive post-buckling, thermal post-buckling and thermo-mechanical post-buckling of perfect and imperfect FGM plates. An iteration process detailed by Liew et al. (2003) and Yang et al. (in press) is used to obtain the post-buckling equilibrium path of the plate.

4. Numerical results

4.1. Comparison study

Prior to the post-buckling analysis of imperfect FGM plates under edge compressive loading and a uniform temperature change, the post-buckling of simply supported, symmetrically cross-ply (0°/90°/0°) square plates ($a/h = 10$) that are made of graphite/epoxy (T300/5028) and subjected to equal biaxial

compression is solved as a sample problem to validate the present formulation and the solution method. The elastic constants are $E_{11} = 25E_{22}$, $G_{12} = G_{13} = 0.5E_{22}$, $G_{23} = 0.2E_{22}$, and $\nu_{12} = 0.28$. The post-buckling equilibrium paths, in the form of nonlinear load–deflection curves, are given in Fig. 2 for both perfect and imperfect plates together with the HSDPT-based perturbation results of Bhimaraddi (1992) for direct comparison. The present results are obtained with the number of nodal lines $N = 15$ and the truncated number of series $M = 5$. Excellent agreement is achieved.

For imperfect plates, the initial geometrical imperfection is assumed to be of the form similar to the deformed shape with an amplitude $\eta = 0.05$. This imperfection is included in the analysis by introducing the relationship

$$w^* = \frac{\eta^* - 1}{2} w$$

into Eqs. (18) and (19). The so-called imperfection parameter $\eta^* = 1.1$ when $\eta = 0.05$.

4.2. Parametric studies

In what follows, parametric studies are undertaken to investigate the post-buckling response of FGM plates with an initial imperfection and subjected to combined mechanical and thermal loads. To this end, nine imperfection modes are involved in the numerical illustrations with parameters

$$\delta_1 = \delta_2 = 0, \mu_1 = \mu_2 = 1, \psi_1 = \psi_2 = 0.5$$

for sine-type imperfection,

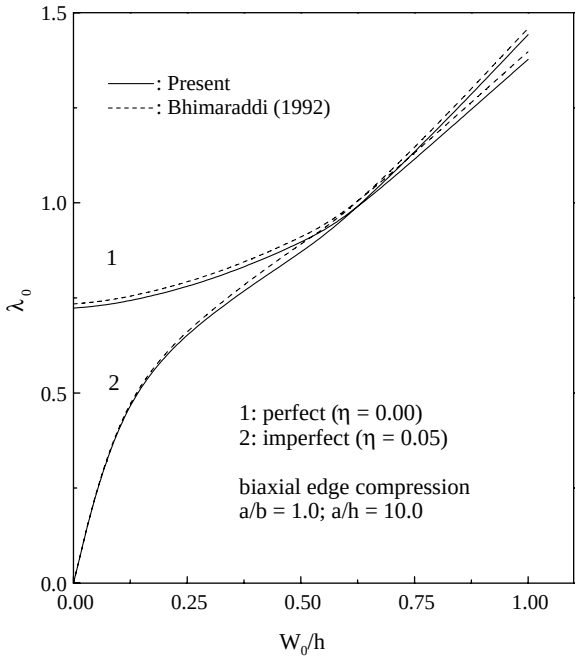

Fig. 2. Comparisons of post-buckling equilibrium paths for a simply supported (0°/90°/0°) square plate under equal biaxial compression.

G1-mode: $\delta_1 = \delta_2 = 0,\ \mu_1 = \mu_2 = 3,\ \psi_1 = \psi_2 = 0.5$
G2-mode: $\delta_1 = \delta_2 = 0,\ \mu_1 = \mu_2 = 5,\ \psi_1 = \psi_2 = 0.5$
G3-mode: $\delta_1 = \delta_2 = 0,\ \mu_1 = \mu_2 = 7,\ \psi_1 = \psi_2 = 0.5$

for global-type imperfections, and

L1-mode: $\delta_1 = 15,\ \mu_1 = 2,\ \psi_1 = 0.25,\ \delta_2 = 0,\ \mu_2 = 1,\ \psi_2 = 0.5$
L2-mode: $\delta_1 = 15,\ \mu_1 = 2,\ \psi_1 = 0.50,\ \delta_2 = 0,\ \mu_2 = 1,\ \psi_2 = 0.5$
L3-mode: $\delta_1 = 15,\ \mu_1 = 2,\ \psi_1 = 0.50,\ \delta_2 = 0,\ \mu_2 = 3,\ \psi_2 = 0.5$
L4-mode: $\delta_1 = 15,\ \mu_1 = 2,\ \psi_1 = 0.50,\ \delta_2 = 0,\ \mu_2 = 5,\ \psi_2 = 0.5$
L5-mode: $\delta_1 = 15,\ \mu_1 = 2,\ \psi_1 = 0.50,\ \delta_2 = 0,\ \mu_2 = 7,\ \psi_2 = 0.5$

for local-type imperfections.

Aluminum (Al) and zirconia (ZrO_2) are chosen as the metallic and ceramic phases of the plate with thermo-elastic material properties:

$$E_m = 70\ \text{GPa}, \nu_\text{m} = 0.3, \alpha_m = 2.3 \times 10^{-5}\ 1/\text{K}, \quad E_c = 151\ \text{GPa}, \nu_c = 0.3, \alpha_c = 1.0 \times 10^{-5}\ 1/\text{K}$$

The post-buckling equilibrium paths, in the form of the dimensionless load parameter $\lambda_0 = p_0 b^2/(4\pi^2 D_0)$ in Figs. 3–8, 10–12 and λ_T in Fig. 9 plotted against the dimensionless additional central deflection W_0/h, are for clamped FGM square plates with volume fraction index $n = 2.0$, side-to-thickness ratio $a/h = 10.0$ and imperfection amplitude $\eta = 0.1$, unless otherwise specified. The plates are compressed by equal biaxial edge forces ($r_x = r_y = 1.0$) in Figs. 3–7, 10–12 or subjected to a uniaxial compression ($r_x \neq 0.0$, $r_y = 0.0$) together with a uniform temperature increase in Figs. 8 and 9. To facilitate the numerical illustration in these figures, the value of D_{11}^* for an isotropic aluminum plate with a thickness $h = 0.01$ m is selected to be the reference

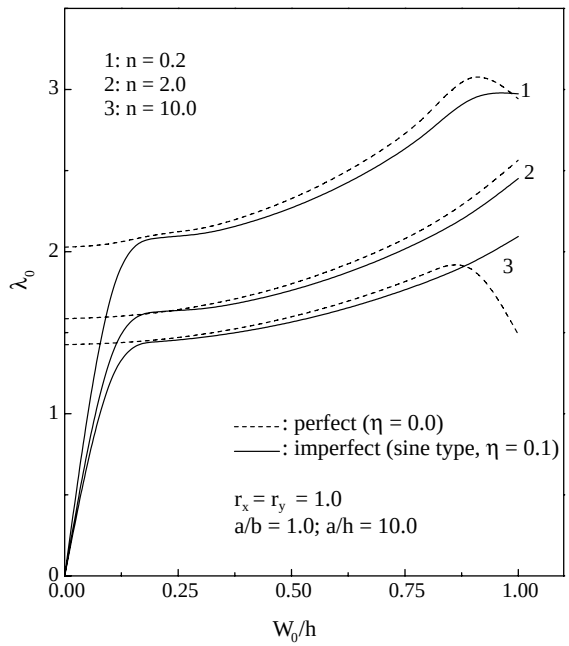

Fig. 3. Compressive post-buckling equilibrium paths for perfect and imperfect clamped functionally graded square plates with varying material compositions.

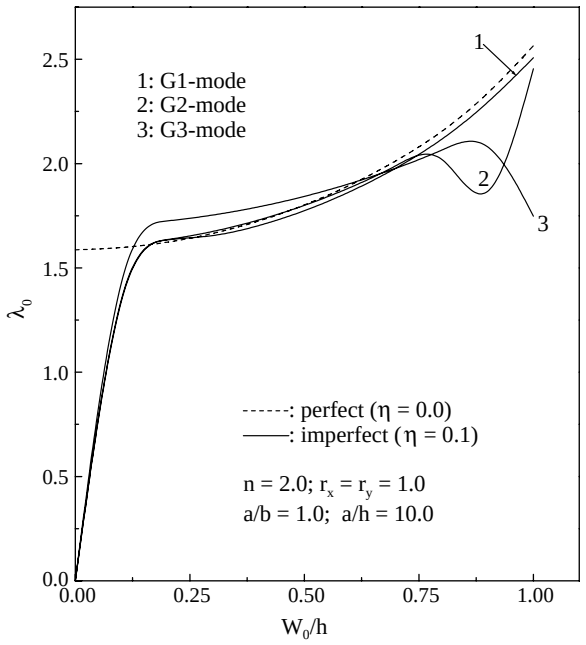

Fig. 4. Compressive post-buckling equilibrium paths for clamped functionally graded square plates with various global imperfections.

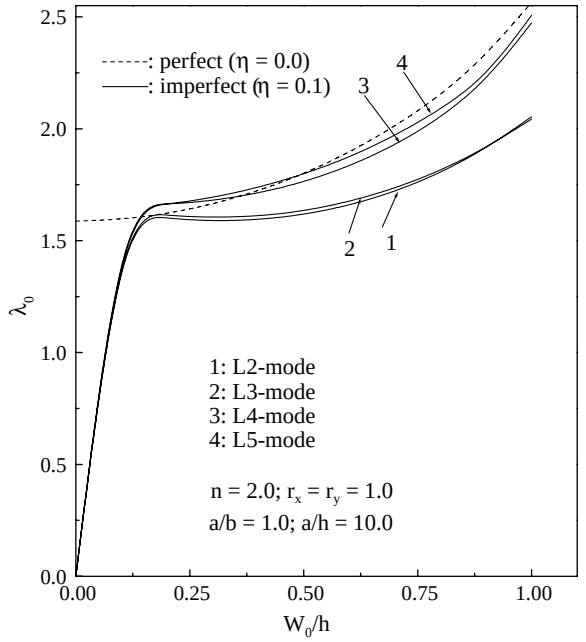

Fig. 5. Compressive post-buckling equilibrium paths for clamped functionally graded square plates with various local imperfections.

stiffness, and is denoted by D_0. The solid lines and the dashed lines represent the results for imperfect plates and perfect plates, respectively, except in Fig. 7.

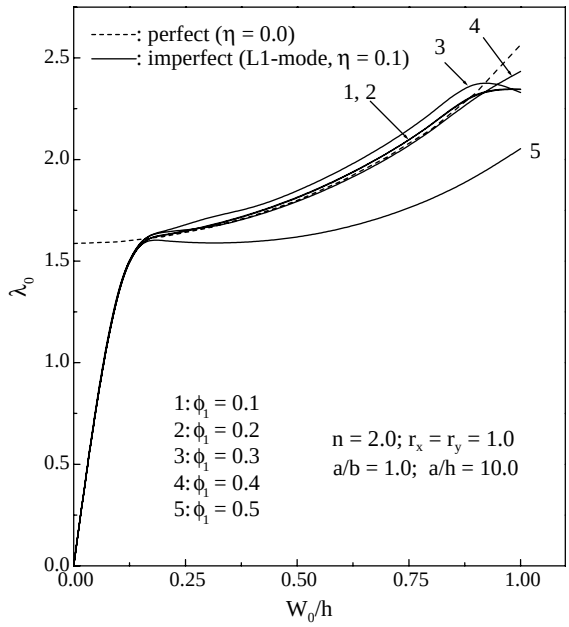

Fig. 6. Compressive post-buckling equilibrium paths for clamped functionally graded square plates with varying locations in local imperfections.

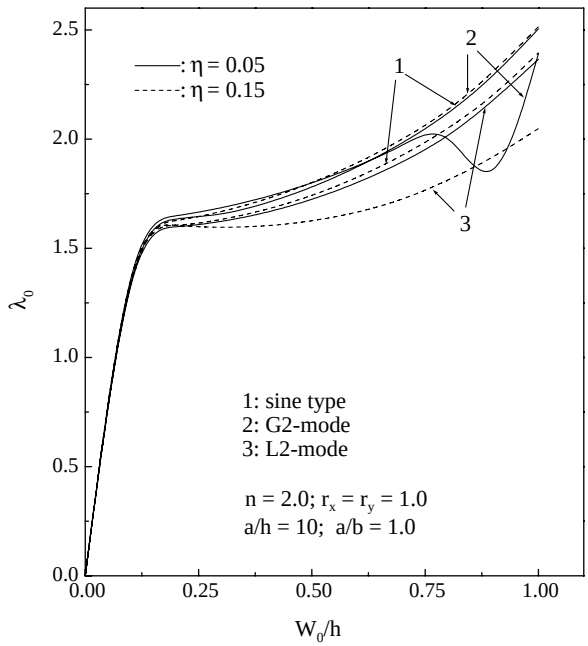

Fig. 7. Compressive post-buckling equilibrium paths for clamped functionally graded square plates with varying imperfection amplitudes.

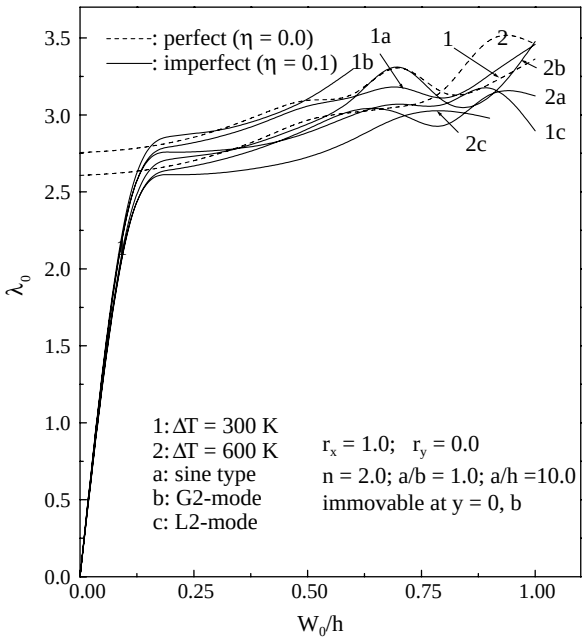

Fig. 8. Thermo-mechanical post-buckling equilibrium paths for clamped functionally graded square plates under constant uniform temperature change.

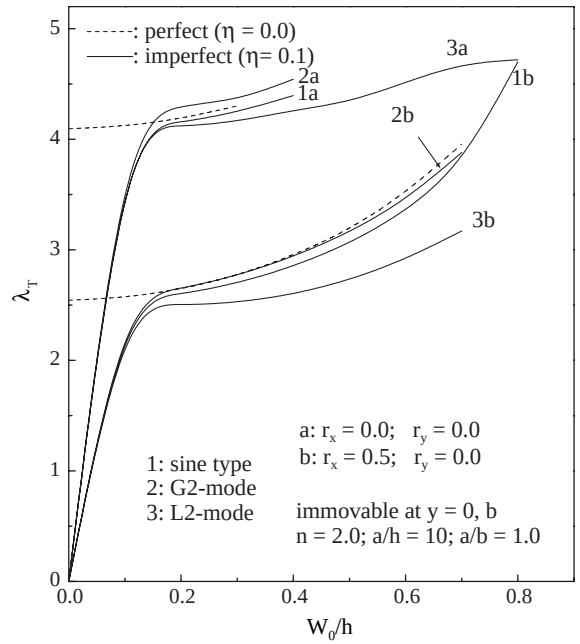

Fig. 9. Thermo-mechanical post-buckling equilibrium paths for clamped functionally graded rectangular plates under different uniaxial edge compression.

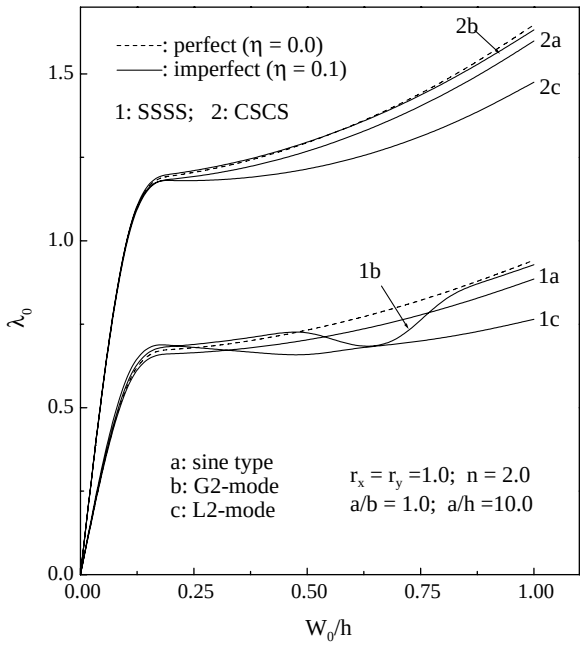

Fig. 10. Compressive post-buckling equilibrium paths for functionally graded square plates with SSSS and CSCS boundary conditions.

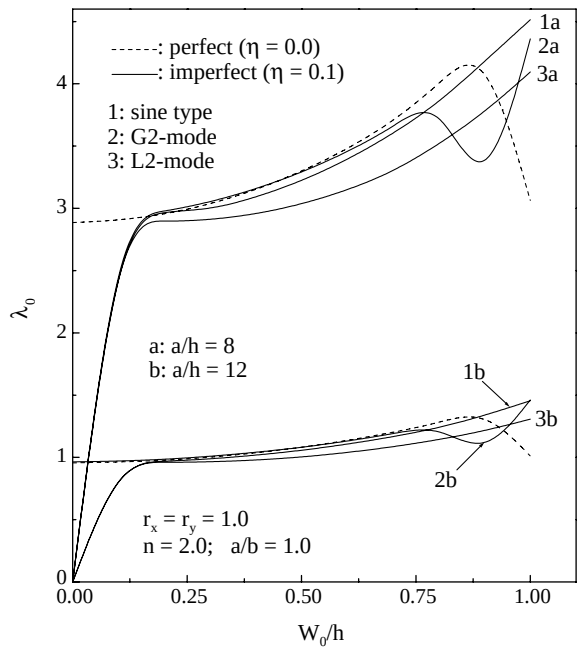

Fig. 11. Compressive post-buckling equilibrium paths for clamped functionally graded square plates with varying side-to-thickness ratios.

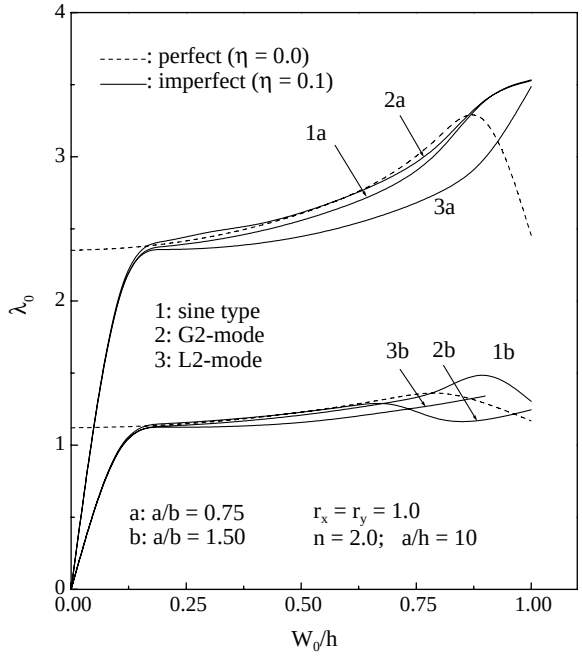

Fig. 12. Compressive post-buckling equilibrium paths for clamped functionally graded rectangular plates with varying aspect ratios.

Fig. 3 shows the compressive post-buckling equilibrium paths of FGM plates with different material compositions ($n = 0.2$, 2.0, 10.0). The sine-mode imperfection is considered in this example. As expected, the post-buckling load-carrying capacity for both perfect and imperfect graded plates increases as the volumetric percentage of the high modulus ZrO_2 increases at a lower volume fraction index n. No obvious effect is observed of the variation in n on the imperfection sensitivity of the post-buckling response. The post-buckling curves of the imperfect plates are slightly lower than their perfect counterparts before $W_0/h \approx 0.9$. A sudden decline in the post-buckling curves of the two perfect plates ($n = 0.2$, 10.0) indicates the possible occurrence of the so-called ''secondary instability''. This phenomenon is also observed in all of the other examples, except for Figs. 5 and 9.

Fig. 4 examines the compressive post-buckling behavior of graded plates with global-type geometric imperfections (G1-, G2- and G3-modes) that are symmetric about the plate center. The half-wave numbers for the G1-, G2- and G3-modes are 3, 5, and 7, respectively. The effect of the half-wave number of globally distributed imperfections on the post-buckling response of graded plates is seen to be not very important. The post-buckling equilibrium path of the imperfect plate with G3-mode imperfection is initially higher than the curve of the perfect plate when $W_0/h = 0.20 \sim 0.70$, but as the load increases it becomes lower and suddenly drops at $W_0/h = 0.9$. The plate with G2-mode imperfection exhibits the typical secondary instability starting from $W_0/h = 0.78$.

The effect of the half-wave number of the imperfection mode on the compressive post-buckling behavior of a graded plate is further studied in Fig. 5 through a comparison of its response sensitivity to local imperfections that are also symmetric with respect to the plate center. For this purpose, L2, L3, L4 and L5 are chosen to be the local imperfection modes in this example and the half-wave numbers are 2 in the x-direction and 1, 3, 5, and 7 in the y-direction. Overall, the post-buckling strength becomes higher as the imperfection half-wave number increases, and the curves of imperfect plates with L4-mode and L5-mode imperfections are close to the curve of the perfect plate. This implies that the post-buckling equilibrium

path tends to be much less affected if the local initial geometrical imperfection has a higher half-wave number.

The post-buckling sensitivity of graded plates to unsymmetrically distributed local imperfections is also investigated. This is undertaken by considering an L1-mode imperfection, the geometric center of which is deviated from the plate center along ξ-axis with varying values of ψ_1 used in Eq. (4). The compressive post-buckling equilibrium paths for five cases of ψ_1 ($\psi_1 = 0.1$, 0.2, 0.3, 0.4, 0.5) are computed and compared in Fig. 6. Note that the unsymmetrical L1-mode virtually becomes a symmetric L2-mode when $\psi_1 = 0.5$. The results show that the post-buckling load-carrying capacity is most weakened by the symmetric imperfection mode that is centered at the plate center. The post-buckling responses of the perfect plate and the imperfect plates with $\psi_1 = 0.1$, 0.2, 0.4 are almost identical, especially before W_0/h approaches somewhere around 0.9.

We next look into the effect of imperfection amplitude on the post-buckling equilibrium paths of graded plates. Fig. 7 displays the compressive post-buckling curves of imperfect graded plates with imperfection amplitudes $\eta = 0.05$ and $\eta = 0.15$, which are denoted by the solid lines and the dashed lines, respectively. The imperfections considered in this example and hereafter in Figs. 8–12 are sine-mode, G2-mode and L2-mode. It can be seen that an increase in the imperfection amplitude lowers the post-buckling equilibrium path for plates with sine type and L2-mode imperfections. This reduction is quite significant for the plate with L2-mode local imperfection. The plate with G2-mode imperfection, however, possesses almost the same post-buckling strength in these two cases before $W_0/h = 0.8$. A secondary instability then takes place beyond this point for the plate with smaller imperfection amplitude ($\eta = 0.05$) and its post-buckling strength becomes much less than that of the plate with greater imperfection amplitude ($\eta = 0.15$).

Fig. 8 shows the thermo-mechanical post-buckling equilibrium paths of perfect and imperfect graded plates subjected to uniaxial compression in the x-axis ($r_x = 1.0$, $r_y = 0.0$) and a constant temperature increment. The plate is allowed to move along the x-axis and restrained against any in-plane displacements in the y-axis. Line groups 1 and 2 represent the results for the cases of $\Delta T = 300$ K and $\Delta T = 600$ K, respectively. The compressive post-buckling behavior of graded plates under a constant temperature change is much more complicated compared with the results obtained in the previous examples where no thermal effect is included. The temperature increment is seen to reduce the post-buckling strength of the imperfect plates, as would be expected. This is because the existence of the thermally induced compressive in-plane stress state results in deterioration in the plate stiffness. It is interesting to note that nearly all of the plates experience secondary instability and for perfect plates in particular, the post-buckling curve at $\Delta T = 600$ K even surpasses the curve at $\Delta T = 300$ K in the larger deflection range ($W_0/h \geqslant 0.8$). The temperature change, however, seems to have very little influence on the sensitivity of post-buckling response to all of the three imperfection modes considered.

Fig. 9 further studies the thermo-mechanical post-buckling behavior of the same plates discussed in Fig. 8 but subjected to another loading case. In this example, the thermo-mechanical load consists of a constant uniaxial compression in the x-axis and an increasing uniform temperature change. Among the two in-plane load cases considered, $r_x = r_y = 0$ indicates that no edge compression is present and the curves in group "a" for this case are virtually the thermal post-buckling equilibrium paths, while $r_x = 0.5$, $r_y = 0$ refers to a case in which the plate is loaded by a combination of a uniform temperature rise and a constant uniaxial compression λ_x that is half of the compressive buckling load of the perfect plate compressed by λ_x only. The presence of edge compression considerably lowers the thermo-mechanical post-buckling curves and makes the plate more sensitive to the initial geometrical imperfection, especially to the L2-mode local imperfection. Unlike the compressive post-buckling results in other examples, many of the nonlinear deflection-temperature curves stop at relatively small deflections, e.g., the post-buckling curves of the thermally loaded perfect plate and imperfect plates containing sine type and G2-mode imperfections, which are much higher than the curves of the thermo-mechanically loaded plates, stop at $W_0/h = 0.3$ and $W_0/h = 0.4$, respectively.

The effects of the boundary condition and the plate geometry are investigated in Figs. 10–12, where the plate is loaded by equal biaxial compression only. No thermal load is included. Fig. 10 shows the post-buckling equilibrium paths of imperfect graded plates with different boundary conditions. "SSSS" refers to a plate simply supported at all edges and "CSCS" refers to a plate simply supported at $x = 0$, 1 and clamped at $y = 0$, 1. The post-buckling curves in all cases have a similar pattern, except that the SSSS plates with G2-mode imperfections exhibits a typical secondary instability in the vicinity of $W_0/h = 0.6$. A comparison of the results in this figure and those for clamped plates shows that the discrepancy between the post-buckling responses of the graded plates with sine-mode, G2-mode and L2-mode imperfections are almost the same, regardless of the different boundary conditions involved. This may lead to the conclusion that the edge supporting condition which considerably influences the post-buckling load-carry capacity does not substantially affect the imperfection sensitivity of the post-buckling behavior of imperfect graded plates.

Figs. 11 and 12 depict the post-buckling equilibrium paths of graded plates with varying side-to-thickness ratios a/h and aspect ratios a/b. Graded plates with $a/h = 8$, 12 and $a/b = 0.75$, 1.50 have been analyzed, with the value of a being kept constant in all cases. Among those considered, the plate with $a/h = 8$ and that with $a/b = 0.75$ have considerably higher post-buckling strength than the other plates. The results also demonstrate that graded plates tend to be more sensitive to geometrical imperfections as the values of a/h and a/b decrease. The post-buckling curves of graded plates with different thicknesses have a similar pattern. But for rectangular graded plates, although the post-buckling curves in three imperfection cases are very close before $W_0/h = 0.62$–0.64, these curves begin to follow a somewhat different way afterwards.

Figs. 7–12 also show that basically, the post-buckling curves of perfect plates and imperfect plates with sine-mode and G2-mode imperfections are not only quite close to each other especially when deflection W_0/h is not large, but are also clearly higher than the curves of locally imperfect plates, which confirms that the post-buckling behavior of graded plates is relatively insensitive to sine-mode and global imperfections but is much more sensitive to locally distributed, symmetric imperfections.

Note that in Figs. 8, 9, 12, some of the post-buckling equilibrium paths stop at certain values of W_0/h, indicating that these plates will lose load-carrying capacity beyond these points.

5. Conclusions

The imperfection sensitivity of the post-buckling behavior of shear deformable FGM plates under uniform edge compression and a uniform temperature change is investigated in this paper by using Reddy's higher-order shear deformation plate theory and a semi-analytical approach. The effects of a wide range of initial geometrical imperfection modes on the post-buckling response are evaluated through parametric studies. The results show that the post-buckling strength is relatively insensitive to sine-mode and global imperfections but is highly sensitive to L2-mode local imperfections that are located at the center of the plate. The effect of a local imperfection becomes much less as its center deviates from the center of the plate. The introduction of edge compression significantly weakens the thermo-mechanical post-buckling load-carrying capacity. An increase in the volume fraction index, the side-to-thickness ratio and the plate aspect ratio also greatly lowers the post-buckling curves, but has an insignificant effect on the imperfection sensitivity of the post-buckling response of the plate.

Acknowledgements

The work described in this paper was funded by a grant from the Research Grants Council of the Hong Kong Special Administrative Region, China (Project No. CityU 1139/04E). The authors are grateful for this financial support.

Appendix A

$$L_{11}(\,) = \gamma_{110}\frac{\partial^4}{\partial\xi^4} + 2\gamma_{112}\beta^2\frac{\partial^4}{\partial\xi^2\partial\zeta^2} + \gamma_{114}\beta^4\frac{\partial^4}{\partial\zeta^4},$$

$$L_{12}(\,) = \gamma_{120}\frac{\partial^3}{\partial\xi^3} + \gamma_{122}\beta^2\frac{\partial^3}{\partial\xi\partial\zeta^2},$$

$$L_{13}(\,) = \gamma_{131}\beta\frac{\partial^3}{\partial\xi^2\partial\zeta} + \gamma_{133}\beta^3\frac{\partial^3}{\partial\zeta^3},$$

$$L_{14}(\,) = \gamma_{140}\frac{\partial^4}{\partial\xi^4} + \gamma_{142}\beta^2\frac{\partial^4}{\partial\xi^2\partial\zeta^2} + \gamma_{144}\frac{\partial^4}{\partial\zeta^4},$$

$$L_{21}(\,) = \frac{\partial^4}{\partial\xi^4} + \gamma_{212}\beta^2\frac{\partial^4}{\partial\xi^2\partial\zeta^2} + \gamma_{214}\beta^4\frac{\partial^4}{\partial\zeta^4},$$

$$L_{22}(\,) = \gamma_{220}\frac{\partial^3}{\partial\xi^3} + \gamma_{222}\beta^2\frac{\partial^3}{\partial\xi\partial\zeta^2}, \quad L_{23}(\,) = \gamma_{231}\beta\frac{\partial^3}{\partial\xi^2\partial\zeta} + \gamma_{233}\beta^3\frac{\partial^3}{\partial\zeta^3},$$

$$L_{24}(\,) = \gamma_{240}\frac{\partial^4}{\partial\xi^4} + \gamma_{242}\beta^2\frac{\partial^4}{\partial\xi^2\partial\zeta^2} + \gamma_{244}\beta^4\frac{\partial^4}{\partial\zeta^4},$$

$$L_{31}(\,) = \gamma_{31}\frac{\partial}{\partial\xi} + \gamma_{310}\frac{\partial^3}{\partial\xi^3} + \gamma_{312}\beta^2\frac{\partial^3}{\partial\xi\partial\zeta^2},$$

$$L_{32}(\,) = \gamma_{31} - \gamma_{320}\frac{\partial^2}{\partial\xi^2} - \gamma_{322}\beta^2\frac{\partial^2}{\partial\zeta^2},$$

$$L_{33}(\,) = \gamma_{331}\beta\frac{\partial^2}{\partial\xi\partial\zeta}, \quad L_{34}(\,) = L_{22}(\,),$$

$$L_{41}(\,) = \gamma_{41}\beta\frac{\partial}{\partial\zeta} + \gamma_{411}\beta\frac{\partial^3}{\partial\xi^2\partial\zeta} + \gamma_{413}\beta^3\frac{\partial^3}{\partial\zeta^3}, \quad L_{42}(\,) = L_{33}(\,),$$

$$L_{43}(\,) = \gamma_{41} - \gamma_{430}\frac{\partial^2}{\partial\xi^2} - \gamma_{432}\beta^2\frac{\partial^2}{\partial\zeta^2}, \quad L_{44}(\,) = L_{23}(\,).$$

Appendix B

The dimensionless quantities in Appendix A are defined as

$$(\gamma_{110},\gamma_{112},\gamma_{114}) = c_1[F^*_{11},(F^*_{12}+F^*_{21}+4F^*_{66})/2,F^*_{22}]/D^*_{11},$$
$$(\gamma_{120},\gamma_{122}) = [(D^*_{11}-c_1F^*_{11}),(D^*_{12}-c_1F^*_{12}+2D^*_{66}-2c_1F^*_{66})]/D^*_{11}$$
$$(\gamma_{131},\gamma_{133}) = [(D^*_{12}-c_1F^*_{21}+2D^*_{66}-2c_1F^*_{66}),(D^*_{22}-c_1F^*_{22})]/D^*_{11},$$
$$(\gamma_{140},\gamma_{142},\gamma_{144}) = c_1[B^*_{21},(B^*_{11}+B^*_{22}-2B^*_{66}),B^*_{12}]/\Delta,$$
$$(\gamma_{212},\gamma_{214}) = [(2A^*_{12}+A^*_{66})/2,A^*_{12}]/A^*_{22},$$
$$(\gamma_{220},\gamma_{222}) = [(B^*_{21}-c_1E^*_{21}),B^*_{11}-B^*_{66}-c_1(E^*_{11}-E^*_{66})]/\Delta,$$
$$(\gamma_{231},\gamma_{233}) = [B^*_{22}-B^*_{66}-c_1(E^*_{22}-E^*_{66}),(B^*_{12}-c_1E^*_{12})]/\Delta,$$
$$(\gamma_{240},\gamma_{242},\gamma_{244}) = c_1[E^*_{21},(E^*_{11}+E^*_{22}-2E^*_{66}),E^*_{12}]/\Delta,$$

$$(\gamma_{310},\gamma_{312}) = c_1[(F^*_{11} - c_1H^*_{11}),(F^*_{21} + 2F^*_{66} - c_1(H^*_{12} + 2H^*_{66}))]/\Delta,$$

$$(\gamma_{320},\gamma_{322},\gamma_{331}) = [(D^*_{11} - 2c_1F^*_{11} + c_1^2H^*_{11}),(D^*_{66} - 2c_1F^*_{66} + c_1^2H^*_{66}),$$
$$D^*_{12} + D^*_{66} - c_1(F^*_{12} + F^*_{21} + 2F^*_{66}) + c_1^2(H^*_{12} + H^*_{66})]/D^*_{11},$$

$$(\gamma_{411},\gamma_{413}) = c_1[F^*_{12} + 2F^*_{66} - c_1(H^*_{12} + 2H^*_{66}),F^*_{22} - c_1H^*_{22}]/\Delta,$$

$$(\gamma_{430},\gamma_{432}) = [(D^*_{66} - 2c_1F^*_{66} + c_1^2H^*_{66}),(D^*_{22} - 2c_1F^*_{22} + c_1^2H^*_{22})]/D^*_{11},$$

$$(\gamma_{31},\gamma_{41}) = [(A^*_{55} - 6c_1D^*_{55} + 9c_1^2F^*_{55}),(A^*_{44} - 6c_1D^*_{44} + 9c_1^2F^*_{44})]/D^*_{11}.$$

References

Bert, C.W., Wang, X., Striz, A.G., 1993. Differential quadrature for static and free vibration analysis of anisotropic plates. International Journal of Solids and Structures 30, 1737–1744.

Bert, C.W., Jang, S.K., Striz, A.G., 1998. Two new approximate methods for analyzing free vibration of structural components. AIAA Journal 26, 612–618.

Bhimaraddi, A., 1992. Buckling and post-buckling behavior of laminated plates using the generalized nonlinear formulation. International Journal of Mechanical Sciences 34, 703–715.

Chen, X.L., Liew, K.M., 2004. Buckling of rectangular functionally graded material plates subjected to nonlinearly distributed in-plane edge loads. Smart Materials and Structures 13, 1430–1437.

Dawe, D.J., Wang, S., Lam, S.S.E., 1995. Finite strip analysis of imperfect laminated plates under end shortening and normal pressure. International Journal for Numerical Methods in Engineering 38, 4193–4205.

Featherston, C.A., 2001. Imperfection sensitivity of flat plates under combined compression and shear. International Journal of Non-Linear Mechanics 36, 249–259.

Feldman, E., Aboudi, J., 1997. Buckling analysis of FGM plates subjected to uniaxial loading. Composite Structures 38, 29–36.

Girish, J., Ramachandra, L.S., 2005. Thermomechanical post-buckling analysis of symmetric and antisymmetric composite plates with imperfections. Composite Structures 67, 453–460.

Hui, D., 1986. Imperfection sensitivity of axially compressed laminated flat plates due to bending–stretching coupling. International Journal of Solids and Structures 22, 13–22.

Ichikawa, K. (Ed.), 2000. Functionally graded materials in the 21st Century: A workshop on trends and forecasts, Japan. Kluwer Academic Publishers.

Javaheri, R., Eslami, M.R., 2002. Thermal buckling of FGM plates based on higher order theory. Journal of Thermal Stresses 25, 603–625.

Kapania, R.K., Yang, T.Y., 1987. Buckling, post-buckling and nonlinear vibrations of imperfect plates. AIAA Journal 25, 1338–1346.

Kitipornchai, S., Yang, J., Liew, K.M., 2004. Semi-analytical solution for nonlinear vibration of laminated FGM plates with geometric imperfections. International Journal of Solids and Structures 41, 2235–2257.

Librescu, L., Lin, W., Nemeth, M.P., Starnes, J.H., 1995. Thermomechanical post-buckling of geometrically imperfect flat and curved panels taking into account tangential edge constraints. Journal of Thermal Stresses 18, 465–482.

Librescu, L., Souza, M.A., 1993. Postbuckling of geometrically imperfect shear-deformable flat panels under combined thermal and compressive edge loadings. Journal of Applied Mechanics—ASME 60, 526–533.

Liew, K.M., Teo, T.M., Han, J.B., 2001. Three-dimensional static solutions of rectangular plates by variant differential quadrature method. International Journal of Mechanical Sciences 43, 1611–1628.

Liew, K.M., Yang, J., Kitipornchai, S., 2003. Postbuckling of the piezoelectric FGM plates subjected to thermo-electro-mechanical loading. International Journal of Solids and Structures 40, 3869–3892.

Liew, K.M., Yang, J., Kitipornchai, S., 2004. Thermal post-buckling of laminated plates comprising FGM with temperature-dependent properties. Journal of Applied Mechanics-ASME 71, 839–850.

Liu, T.H., Lam, S.S.E., 2001. Finite strip analysis of laminated plates with general initial imperfection under end shortening. Engineering Structures 23, 673–686.

Ma, L.S., Wang, T.J., 2003a. Axisymmetric post-buckling of a functionally graded circular plate subjected to uniformly distributed radial compression. Materials Science Forum 423-424, 719–724.

Ma, L.S., Wang, T.J., 2003b. Nonlinear bending and post-buckling of a functionally graded circular plate under mechanical and thermal loadings. International Journal of Solids and Structures 40, 3311–3330.

Morimoto, T., Tanigawa, Y., Kawamura, R., 2003. Thermal buckling analysis of inhomogeneous rectangular plate due to uniform heat supply. Journal of Thermal Stresses 26, 1151–1170.

Na, K.S., Kim, J.H., 2004. Three-dimensional thermal buckling analysis of functionally graded materials. Composites Part B: Engineering 35, 429–437.

Najafizadeh, M.M., Heydari, H.R., 2004. Thermal buckling of functionally graded circular plates based on higher order shear deformation plate theory. European Journal of Mechanics-A/Solids 23, 1085–1100.

Reddy, J.N., 1984. A refined nonlinear theory of plates with transverse shear deformation. International Journal of Solids and Structures 20, 881–896.

Shen, H.S., 1998. Thermomechanical post-buckling analysis of imperfect laminated plates using a higher-order shear-deformation theory. Computers & Structures 66, 395–409.

Shen, H.S., 1999. Thermal post-buckling of imperfect shear-deformable laminated plates on two-parameter elastic foundations. Mechanics of Composite Materials and Structures 6, 207–228.

Shen, H.S., 2000. Thermomechanical post-buckling of imperfect shear deformable laminated plates on elastic foundations. Computer Methods in Applied Mechanics and Engineering 189, 761–784.

Shen, H.S., 2001. Thermal post-buckling behavior of imperfect shear deformable laminated plates with temperature-dependent properties. Computer Methods in Applied Mechanics and Engineering 290, 5377–5390.

Shen, H.S., Williams, F.W., 1997. Thermomechanical post-buckling analysis of imperfect laminated plates on softening nonlinear elastic foundations. Composite Structures 40, 55–66.

Wadee, M.A., 2000. Effects of periodic and localized imperfections on struts on nonlinear foundations and compression sandwich panels. International Journal of Solids and Structures 37, 1191–1209.

Woo, J., Meguid, S.A., Liew, K.M., 2003. Thermomechanical post-buckling analysis of FGM plates and shallow cylindrical shells. Acta Mechanica 165, 99–115.

Yamaki, N., 1959. Postbuckling behavior of rectangular plates with small initial curvature loaded in edge compression. Journal of Applied Mechanics-ASME 26, 407–414.

Yang, J., Liew, K.M., Kitipornchai, S., 2004. Dynamic stability of laminated FGM plates based on higher-order shear deformation theory. Computational Mechanics 33, 305–315.

Yang, J., Liew, K.M., Kitipornchai, S., 2005. Second-order statistics of the elastic buckling of functionally graded rectangular plates. Composites Sciences and Technology 65, 1165–1175.

Yang, J., Liew, K.M., Wu, Y.-F., Kitipornchai, S., Thermo-mechanical post-buckling of FGM cylindrical panels with temperature-dependent properties. International Journal of Solids and Structures, in press, doi:10.1016/j.ijsolstr.2005.04.001.

Yang, J., Shen, H.S., 2003. Non-linear analysis of FGM plates under transverse and in-plane loads. International Journal of Non-Linear Mechanics 38, 467–482.

Yang, J., Shen, H.S., Zhang, L., 2001. Nonlinear local response of foam-filled sandwich plates with laminated faces under combined transverse and in-plane loads. Composite Structures 52, 137–148.

Yang, J., Zhang, L., 2000. Nonlinear analysis of imperfect laminated thin plates under transverse and in-plane loads and resting on an elastic foundation by a semi-analytical approach. Thin-Walled Structures 38, 195–227.

Zou, G.P., Qiao, P.Z., 2002. Higher-order finite strip method for post-buckling analysis of imperfect composite plates. Journal of Engineering Mechanics-ASCE 128, 1008–1015.

Zou, G.P., Lam, S.S.E., 2003. Post-buckling analysis of imperfect laminates using finite strips based on a higher-order plate theory. International Journal for Numerical Methods in Engineering 56, 2265–2278.